

L1₂-Strengthened Cobalt-Base Superalloys

Akane Suzuki,¹ Haruyuki Inui,² and Tresa M. Pollock³

¹Ceramic & Metallurgy Technologies, GE Global Research, Niskayuna, New York 12309;
email: suzukia@ge.com

²Department of Materials Science and Engineering, Kyoto University, Kyoto 606-8501, Japan;
email: inui.haruyuki.3z@kyoto-u.ac.jp

³Materials Department, University of California, Santa Barbara, California 93106;
email: pollock@engineering.ucsb.edu

Ann. Rev. Mater. Res. 2015. 45:345–68

First published online as a Review in Advance on
February 26, 2015

The *Annual Review of Materials Research* is online at
matsci.annualreviews.org

This article's doi:
10.1146/annurev-matsci-070214-021043

Copyright © 2015 by Annual Reviews.
All rights reserved

Keyword

phase stability, high-temperature deformation, dislocation, planar defects, oxidation

Abstract

The discovery of the γ' -Co₃(Al,W) phase with an L1₂ structure provided Co-base alloys with a new strengthening mechanism, enabling a new class of high-temperature material: Co-base superalloys. This review discusses the current understanding of the phase stability, deformation, and oxidation behaviors of γ' single-phase and $\gamma + \gamma'$ two-phase alloys in comparison with Ni-base γ' -L1₂ phase and $\gamma + \gamma'$ superalloys. Relatively low stacking fault energies and phase stability of the γ' phase compared with those in Ni-base alloys are responsible for the unique deformation behaviors observed in Co-base γ' and $\gamma + \gamma'$ alloys. Controlling energies of planar defects, such as stacking faults and antiphase boundaries, by alloying is critical for alloy development. Experimental and density functional theory studies indicate that additions of Ta, Ti, Nb, Hf, and Ni are effective in simultaneously increasing the phase stability and stacking fault energy of γ' -Co₃(Al,W), thus improving the high-temperature strength of Co-base γ' phase and $\gamma + \gamma'$ two-phase superalloys.

1. INTRODUCTION

The discovery of the γ' - $\text{Co}_3(\text{Al},\text{W})$ phase in the Co-Al-W ternary alloy system by Sato et al. (1) began a new era in high-temperature alloy development history. With precipitation strengthening by the γ' phase with an ordered $\text{L}1_2$ structure, Co-base alloys have demonstrated increased high-temperature strength compared with that of conventional Co-base alloys (1–3). **Table 1** shows nominal compositions of representative γ' -strengthened and conventional Co-base alloys. The γ' - $\text{Co}_3(\text{Al},\text{W})$ phase coherently precipitates with a cuboidal morphology in the solid-solution γ -Co (fcc structure) matrix phase (**Figure 1**) due to the relatively small lattice misfit between the γ and γ' phases (1), resulting in a $\gamma + \gamma'$ two-phase microstructure with a regular array of cuboidal γ' precipitates, which resembles the microstructures of Ni-base superalloys strengthened by γ' - Ni_3Al ($\text{L}1_2$) precipitates. To date, Ni-base superalloys have been widely used in applications that require high-temperature mechanical and environmental capabilities, such as aircraft engines and land-based power generation gas turbines, as well as nuclear power and chemical plants (4–6). In contrast, applications of conventional Co-base alloys have been limited to stationary components, such as vanes and combustors, due to a lack of effective high-temperature strengthening mechanisms (7, 8).

Novel $\gamma + \gamma'$ Co-base superalloys have been attracting tremendous interest because they could provide unique solutions to the limitations that Ni-base superalloys face: temperature capability and balance of properties. For gas turbine component applications, there have been consistent demands to increase the metal temperature capability to achieve improved fuel efficiency. Ni-base superalloys have been evolved by (*a*) tailoring the alloy chemistry to improve the stability and properties of phases and (*b*) improving material processes to optimize structure and minimize defects (4–6, 9). The blades in the early stages of the gas turbines are typically single crystals made of advanced Ni-base superalloys consisting of more than 10 elements, including large amounts (up to 11 wt% in total) of rare refractory elements such as Re and Ru (5, 6, 10). A comparison of 1,000-h creep rupture capability of various Ni-base superalloys shows a clear correlation with the γ' -solvus temperature (**Figure 2**) (5, 11), which indicates that a higher γ' -solvus temperature to retain a high volume fraction of the γ' phase is one requirement for better creep resistance. However, the γ' -solvus temperatures of Ni-base superalloys are approaching their limit, i.e., their melting temperatures. In contrast, γ' -strengthened Co-base alloys have a higher upper limit, as their melting temperatures are higher than those of Ni-base superalloys by greater than 50–150°C (12). Their higher melting temperatures are inherent in the higher melting temperature of pure Co compared with that of pure Ni. In wrought Ni-base superalloys—for example, alloys for turbine disk applications—achieving a balance of strength and environmental resistance has been a challenge (13–15). Increased amounts of alloying additions have been made to strengthen γ and γ' phases by reducing Cr, which is an essential element for maintaining oxidation resistance, especially during fatigue crack growth. The new Co-base alloys can take advantage of the γ' -strengthening mechanism and better environmental resistance inherent in conventional Co-base alloys (7, 8). Furthermore, Co-base alloys show superior corrosion resistance, wear resistance, and weldability compared with Ni-base superalloys (7, 8), which may enable Co-base superalloys to have unique combinations of high-temperature strength and other properties inherent in the Co-base alloy system.

Since the discovery of the γ' - $\text{Co}_3(\text{Al},\text{W})$ phase in 2006, significant efforts have been made to understand the thermodynamic, physical, mechanical, and environmental properties of the γ' phase and the γ' -strengthened Co-base superalloys, mainly in comparison with Ni-base superalloys. This review discusses the current understanding of the Co-base superalloy system, including phase stability, deformation behavior, high-temperature mechanical capability, and oxidation behavior. The challenges to overcome and future research needs are also discussed.

Table 1 Nominal compositions of alloys investigated and representative Co- and Ni-base alloys for comparison

Alloy	Description	Nominal composition (wt%)														
		Co	Ni	Al	W	Ta	Ti	Cr	Mo	Fe	Mn	Si	C	B	Zr	Hf
Co-base γ + γ' superalloys																
Co-9Al-9W	Low γ' fraction	Bal.		3.7	24.6											
Co-9Al-11W	High γ' fraction	Bal.		3.7	28.4											
Co-12Al-11W	Near γ' single phase	Bal.		4.7	29.4											
Co-9Al-10W-7Ta	Stable γ'	Bal.		3.4	25.4	5.1										
Co-8Al-8W-1.5Ta-4.5Cr	Stable γ' , oxidation	Bal.		3.1	21.2	4		3.5								
Co-7Al-8W-6Ti	Stable γ'	Bal.		2.7	22.5		4.5									
Co-10Ni-9Al-9W-0.06C-0.01B	Co-Ni base	Bal.	8.7	3.7	24.6									0.001	0.002	
Co-20Ni-10Al-6W-6Cr-2Ta	Co-Ni base	Bal.	26	4	17.5	6.6		5								
Conventional Co-base alloys																
Haynes 188	Wrought alloy		22		14			22		<3	<1.5	0.35	0.1	<0.015		
L605	Wrought alloy		10		15			20		<3	1.5	<0.4	0.1			
FSX414	Cast alloy		10		7			29		<2	<1	<1	0.25			
Ni-base single-crystal superalloy																
René N4	First generation	7.5	Bal.	4.2	6	5	3.5	10	1.5			0.05	0.004	0.15	0.5Nb	
René N5	Second generation	7.5	Bal.	6.2	5	6.5		7	1.5			0.05	0.004	0.15	3Re	
Ni-base polycrystal superalloy																
MarM247	Cast		10	Bal.	5.5	10	3	1	8.2	0.6		0.16	0.015	0.05	1.5	
IN713C	Cast			Bal.	5.8			0.7	13.5	4.5		0.1	0.01	0.06	2Nb	
IN100	Cast or wrought	15	Bal.	5.5			4.75	10	3			0.16	0.015	0.04	0.8V	

Bal. denotes balance. Blank cells denote zero (the alloy does not contain the element).

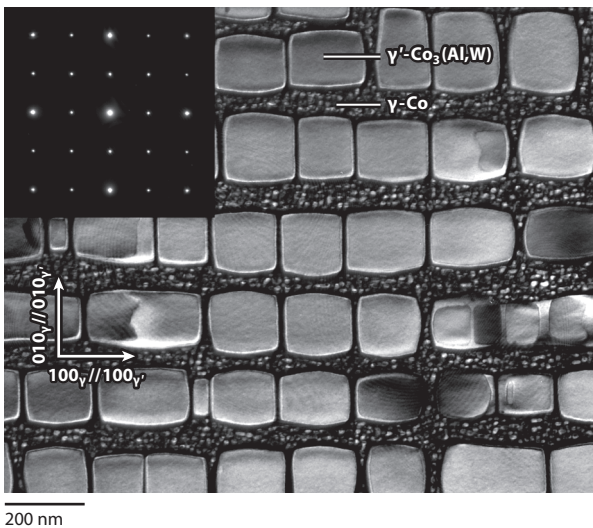


Figure 1

Transmission electron micrograph (dark-field image) of a Co-9Al-9W alloy showing coherent cuboidal γ' - $\text{Co}_3(\text{Al},\text{W})$ (L_1_2 structure) precipitates formed in the solid-solution γ - Co (fcc structure) matrix phase. The specimen was homogenized at 1,350°C for 12 h, followed by aging at 900°C for 150 h. Adapted from Reference 3 with permission.

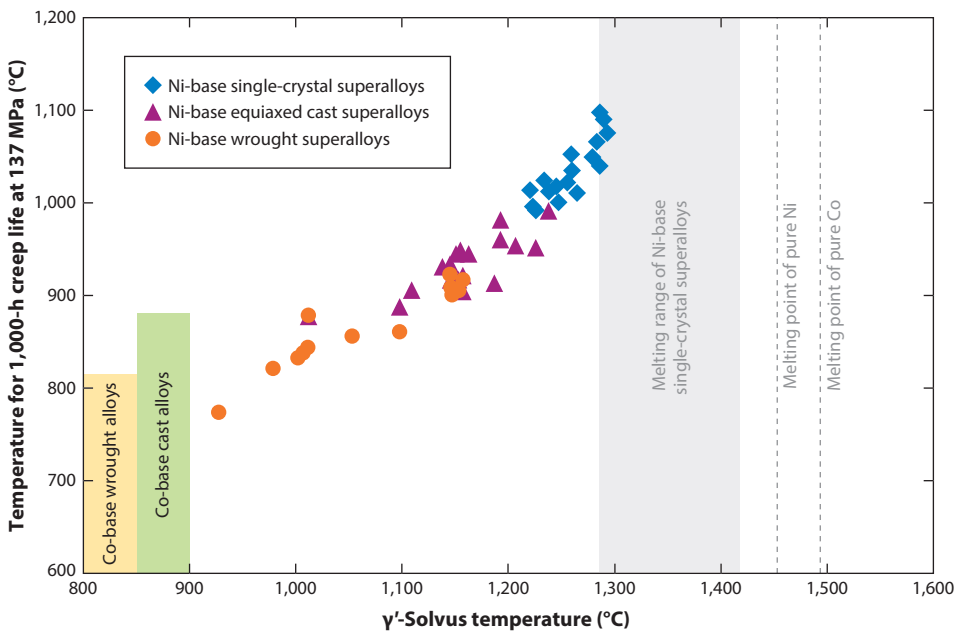


Figure 2

1,000-h creep rupture capability of single-crystal, equiaxed cast and wrought Ni-base superalloys as a function of γ' -solvus temperature in comparison with that of conventional Co-base cast and wrought alloys. Data from References 5, 7, 8, and 11.

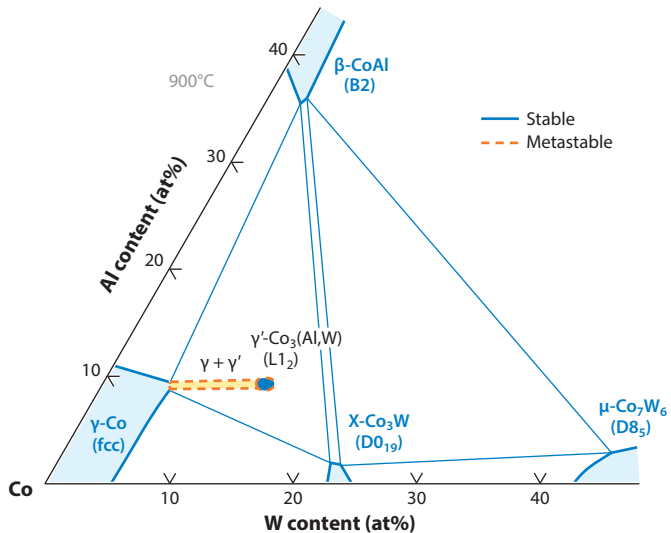


Figure 3

Isothermal section of the Co-Al-W ternary system at 900°C, showing both stable and metastable phase boundaries. Adapted from Reference 17 with permission.

2. STABILITY OF THE γ' -CO₃(AL,W) PHASE

2.1. The Co-Al-W Ternary System

The γ' -CO₃(AL,W) phase was originally reported as an equilibrium phase at 900°C in the Co-Al-W ternary system, having a $\gamma + \gamma'$ two-phase region (1). However, a recent study by Kobayashi et al. (16) revealed that the γ' phase is metastable and that the γ -Co phase is in equilibrium with the β -CoAl (B2) and χ -CO₃W (D0₁₉) phases after extended aging at 900°C for 2,000 h. **Figure 3** shows the Co-Al-W isothermal section at 900°C showing both stable and metastable phase boundaries (17). There is a narrow $\gamma + \gamma'$ metastable two-phase region, and alloys in the $\gamma + \gamma'$ region eventually decompose into γ -Co, B2, and D0₁₉ phases, although the kinetics are extremely slow (16, 18). In addition, the CO₂W Laves phase was recently observed in Co-Al-W ternary alloys at 1,000°C in equilibrium with the B2, μ -CO₇W₆ (D8₅), and γ -Co phases (19). These observations indicate the remaining uncertainty regarding the Co-Al-W ternary-phase equilibria. The development of a validated thermodynamic database for the Co-Al-W ternary- and higher-order systems is critical for future alloy design.

Density functional theory (DFT) calculations (20–22) have addressed the issue of the stability of the γ' -CO₃(AL,W) (L1₂) phase. At 0 K, the stable structure in the ternary Co-Al-W system (the global convex hull) is composed of a three-phase mixture of B2, ε -Co (hcp), and D0₁₉ (**Figure 4**). The experimentally observed existence of the γ' -CO₃(AL,W) (L1₂) phase at finite temperatures indicates that vibrational, configurational, and/or electronic contributions to entropy are crucial to stabilizing the ternary compound at elevated temperatures. Additionally, for pure Co, the contribution of magnetic excitations is important to stabilization of the γ -Co (fcc) phase at elevated temperatures (23). Thus, incorporating the effects of magnetism into first-principles calculations may also be important. Indeed, recent finite-temperature calculations that include these effects demonstrate the stability of the γ' phase above 600°C, with the most significant contributions coming from vibrational entropy (22). The roles of vacancies and antisite defects remain to be

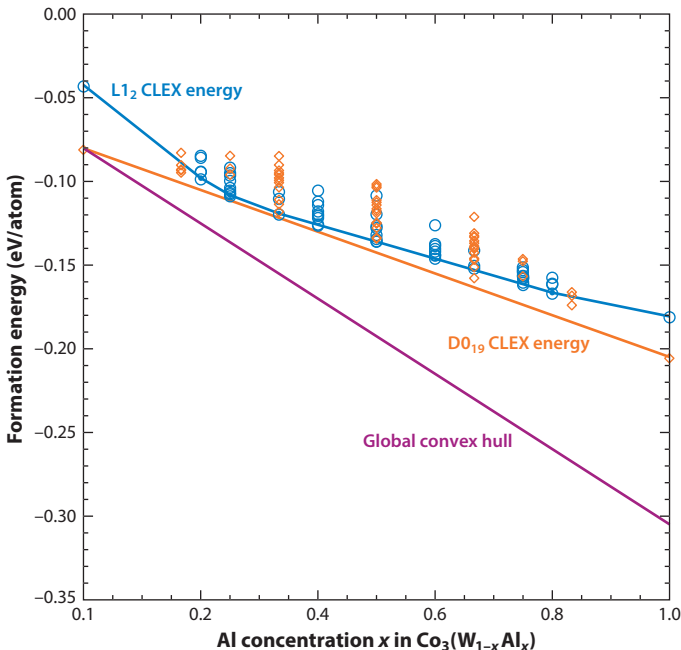


Figure 4

Formation energies of ternary phases derived from L1_2 (blue circles) and from $\text{D}0_{19}$ (orange diamonds) along the pseudobinary $\text{Co}_3(\text{W}_{1-x}\text{Al}_x)$ composition axis. The blue and orange lines denote cluster expansion (CLEX) energies of L1_2 and $\text{D}0_{19}$. The lower purple line (global convex hull) shows the energy of phase separation into a ternary mixture of ε -Co (hcp), β -CoAl (B2), and χ - Co_3W ($\text{D}0_{19}$).

studied in detail. Additionally, as discussed further in Section 4, DFT calculations have also demonstrated an important role of quaternary- and higher-order alloying additions in defect energies and stability of the γ' phase (24, 25).

2.2. Alloying Effect on the Stability of the γ' - $\text{Co}_3(\text{Al},\text{W})$ Phase

The metastable ternary γ' - $\text{Co}_3(\text{Al},\text{W})$ phase becomes a stable phase by additions of γ' -stabilizing elements, such as Ti, Ta, and Hf (26, 27). The effectiveness of alloying elements in stabilizing the γ' phase was compared using the change in the γ' -solvus temperature. In the Co-Al-W ternary system, the metastable γ' -solvus temperature is not high compared with the γ' -solvus temperatures of Ni-base superalloys: only 1,033°C in a Co-9Al-11W alloy that has a high volume fraction of the γ' phase (79% at 900°C) (3). **Figure 5a** shows the increase in the γ' -solvus temperatures per atomic percent quaternary elemental additions ($\Delta T_{\gamma'\text{-solvus}}$) when alloying additions were made by substituting for Co in Co-Al-W ternary alloys (3, 17, 28–33). The most effective element is Ta, followed by Ti, Nb, W, and Hf. An addition of 1-at% Ta increases the γ' -solvus temperature by 45°C. Among the 3d transition metals, Ti has the highest $\Delta T_{\gamma'\text{-solvus}}$. Additions of V and Ni have a slightly positive effect, whereas additions of Cr, Mn, and Fe have a negative effect. According to the elemental partitioning study by Omori et al. (17), the γ' -stabilizing elements tend to partition to the γ' phase against the γ phase, and the γ' -destabilizing elements show the opposite partitioning behaviors (**Figure 5b**). **Figure 6** shows the changes in the γ' -solvus temperatures with additions of Ni, Cr, and Fe, by substituting for Co (31–34). Both Cr and Fe destabilize the γ' phase, and

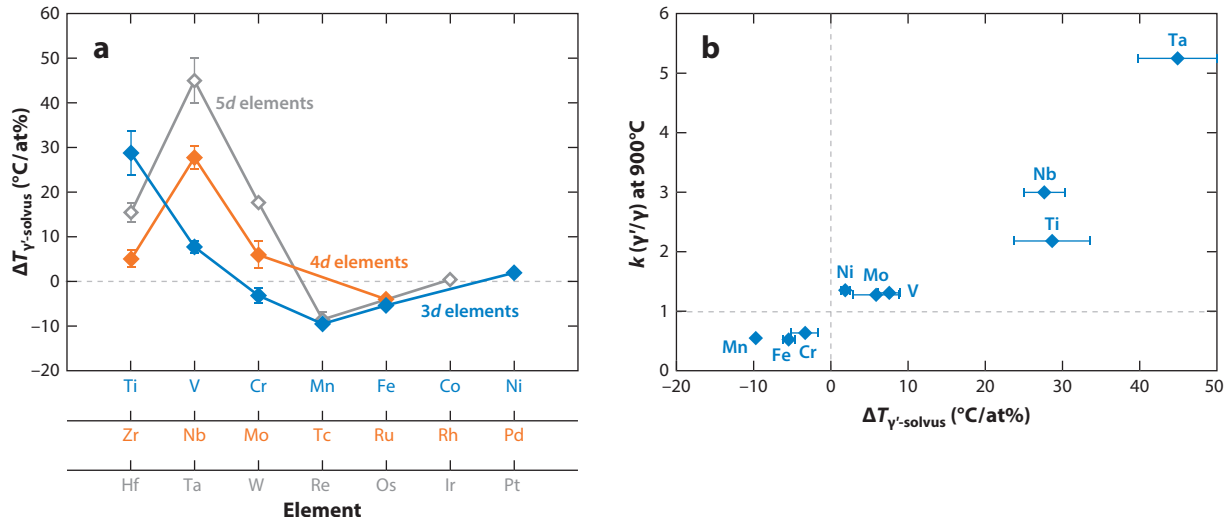


Figure 5

(a) Changes in γ' -solvus temperature ($\Delta T_{\gamma'\text{-solvus}}$) per 1-at% addition of transition metal elements. Data from References 3, 17, and 28–33. (b) Correlation between elemental partitioning behavior (17) and $\Delta T_{\gamma'\text{-solvus}}$ of the alloying elements.

the γ' -solvus temperature is reduced by more than 100°C by adding 20 at% of either element. Also noteworthy is that the $\gamma + \gamma'$ two-phase field is continuous between the Co-Al-W and Ni-Al-W ternary systems (32). The γ' -solvus temperature is increased with additions of Ni, as shown by thermodynamic database and differential scanning calorimetry experiments (Figure 6) (32, 34). The increment by additions of Ni is approximately 200°C due to the large solubility of Ni, although its contribution is small on a per-atomic-percent basis. The propensity for Ni to increase

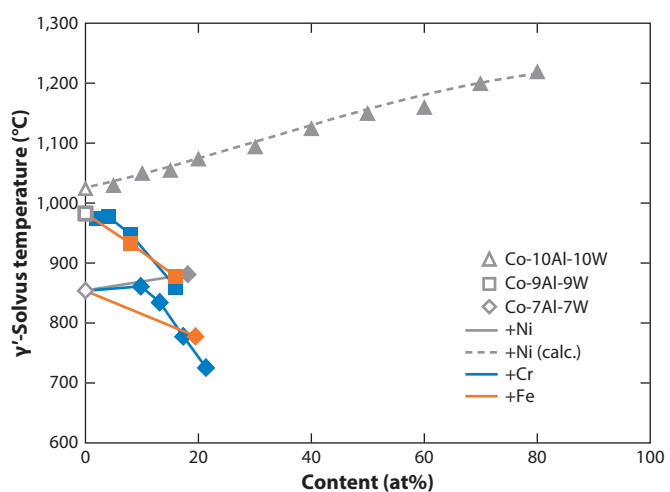


Figure 6

Changes in γ' -solvus temperature by additions of large amounts of Ni, Cr, and Fe in Co-Al-W ternary alloys. Co-10Al-10W data are from Reference 32, Co-9Al-9W data are from Reference 31, Co-7Al-7W data are from Reference 33, and +Ni (calculated) data are from Reference 34.

Table 2 Single-crystal and polycrystalline elastic constants and elastic anisotropy parameters of Co₃(Al,W) in comparison with Ni₃(Al,Ta) (20, 35–37)

	Temperature (K)	Single-crystal elastic constants			Polycrystalline elastic constants				Elastic anisotropy parameters			
		<i>c</i> ₁₁ (GPa)	<i>c</i> ₁₂ (GPa)	<i>c</i> ₄₄ (GPa)	<i>B</i> _h (GPa)	<i>G</i> _h (GPa)	<i>E</i> _h (GPa)	<i>v</i>	<i>A</i>	<i>E</i> ₁₁₁ / <i>E</i> ₁₀₀	<i>c</i> ₁₂ – <i>c</i> ₄₄ (GPa)	<i>G</i> _h / <i>B</i> _h
Co ₃ (Al,W) experiment (35)	5	271	172	162	205	101	260	0.289	3.26	2.8	10	0.493
Co ₃ (Al,W) calculation (36)	0	363	190	212	248	148	370	0.251	2.45	2.13	-22	0.585
Co ₃ (Al,W) calculation (20)	0	264	162	153	196	99	253	0.282	2.89	2.59	9	0.503
Co ₃ (Al,W) calculation (37)	0	301	169	172	213	117	297	0.268	2.61	2.27	-2.7	0.549
Ni ₃ (Al,Ta) experiment (35)	5	238	154	130	182	83	216	0.303	3.19	2.69	24	0.455

the γ' -solvus suggests a large potential alloy design space intermediate to that of conventional Co alloys and that of conventional Ni alloys.

3. MECHANICAL BEHAVIOR OF THE γ' -CO₃(AL,W) PHASE

3.1. Elastic Properties of the γ' -Co₃(Al,W) Phase

Comparison of elastic properties of the γ' -Co₃(Al,W) phase with those of the Ni-base L1₂ compound Ni₃(Al,Ta) indicates that the γ' -Co₃(Al,W) phase is elastically stiffer and more anisotropic than the Ni-base L1₂ phase. **Table 2** summarizes the elastic properties measured at liquid-He temperature and calculated at 0 K (20, 35–37). Elastic constants of single-crystal Co₃(Al,W) are larger than those of Ni₃(Al,Ta) by 15–25% (35). Although first-principles calculations made for Co₃(Al,W) originally indicated considerably high elastic constants (36), the recent results (20, 37) are consistent with the experimental measurements (35). The bulk (*B*_h), shear (*G*_h), and Young's (*E*_h) moduli evaluated for Co₃(Al,W) from the single-crystal elastic constants by Hill's method show a similar trend. γ' -Co₃(Al,W) has a smaller Poisson's ratio and lower Cauchy pressure, which is defined as *c*₁₂ – *c*₄₄ for crystals with cubic symmetry, than does Ni₃(Al,Ta). The smaller Poisson's ratio and lower Cauchy pressure are indicative of more significant directionality of atomic bonding in Co₃(Al,W) than in Ni₃(Al,Ta) and is consistent with the result of first-principles calculations that predict strong covalent bonding between Co and W atoms (37, 38). However, according to Pugh's criterion (39), Co₃(Al,W) is considered ductile because *G*_h/*B*_h of Co₃(Al,W) is far less than 0.57, above which the material of concern is regarded as a brittle material. Although Ni₃(Al,Ta) has lower *G*_h/*B*_h, Co₃(Al,W) is expected to be sufficiently ductile to be practically used as the constituent phase in Co-base superalloys. In fact, a Co-12Al-11W polycrystalline alloy with near γ' single-phase structure exhibits 28% tensile elongation in air at room temperature (40). Comparison of the anisotropic factor [*A* = *2c*₄₄/(*c*₁₁ – *c*₁₂)] and *E*₁₁₁/*E*₁₀₀ suggests that Co₃(Al,W) is more elastically anisotropic than Ni₃(Al,Ta). A high *E*₁₁₁/*E*₁₀₀ is energetically beneficial to the formation of cuboidal L1₂ precipitates faceted parallel to {100} in the γ + γ' two-phase

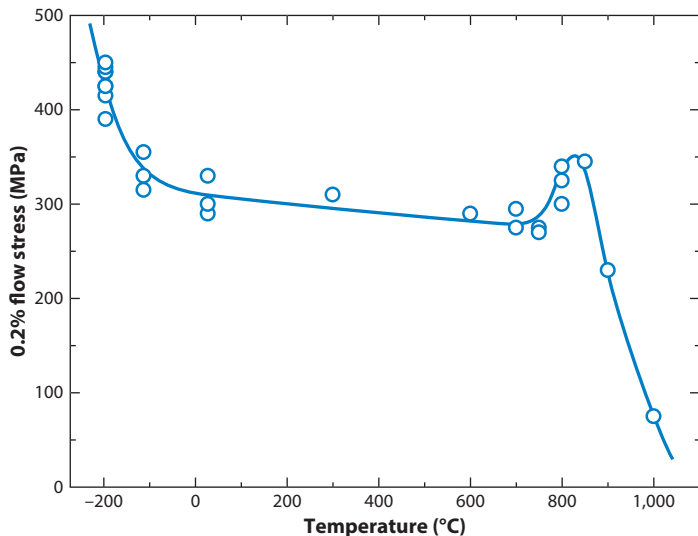


Figure 7

Temperature dependence of the yield stress of a polycrystalline Co-12Al-11W alloy. Adapted from Reference 43 with permission.

microstructure. In addition, large c_{ij} increases the driving force to form cuboidal precipitates aligned parallel to $\langle 100 \rangle$ in the γ phase. Therefore, compared with conventional Ni-base superalloys, Co-base superalloys can more easily form two-phase microstructures containing well-aligned cuboidal γ' precipitates. This tendency may lead to the expectation of better high-temperature properties for Co-base superalloys in view of the formation of raft microstructures.

3.2. Deformation Behavior of γ' - $\text{Co}_3(\text{Al},\text{W})$ Polycrystals

The deformation mechanisms and the temperature dependence of yield stress of $\text{Co}_3(\text{Al},\text{W})$ are quite different from those of Ni_3Al -base $\text{L}1_2$ compounds, in which the yield stress starts to increase anomalously with the increase in temperature from a low temperature (in a range from liquid- N_2 temperature to room temperature, depending on alloy chemistry) with the motion of antiphase boundary (APB)-coupled dislocations with \mathbf{b} (Burgers vector) = $1/2\langle 110 \rangle$ (41, 42). The yield stress of $\text{Co}_3(\text{Al},\text{W})$ polycrystals (Co-12Al-11W) rapidly decreases at low temperatures (up to room temperature), plateaus (up to 680°C), increases anomalously with an increase in temperature in a narrow temperature range from 680°C to 830°C, and then again rapidly decreases at high temperatures (43), as shown in Figure 7. Slip occurs exclusively on $\{111\}$ at all temperatures. The temperature dependence of the yield stress observed in $\text{Co}_3(\text{Al},\text{W})$ is similar to that of Co_3Ti (44) in terms of the appearance of the rapid decrease and the yield stress anomaly at low and high temperatures, respectively, as Miura et al. (45) pointed out. However, compared with the case for Co_3Ti , the onset temperature for the yield stress anomaly is considerably higher, and the temperature range of the anomaly is considerably narrower.

The rapid decrease in yield stress observed at low temperatures in $\text{L}1_2$ compounds such as Co_3Ti (44) and Pt_3Al (46) is usually interpreted in terms of the thermally activated glide of superlattice intrinsic stacking fault (SISF)-coupled dislocation partials ($\mathbf{b} = 1/3\langle 112 \rangle$) whose core is believed to be nonplanar and hence subject to lattice friction (47). However, dislocations observed in $\text{Co}_3(\text{Al},\text{W})$ in this temperature range are usually smoothly curved on the (111) slip

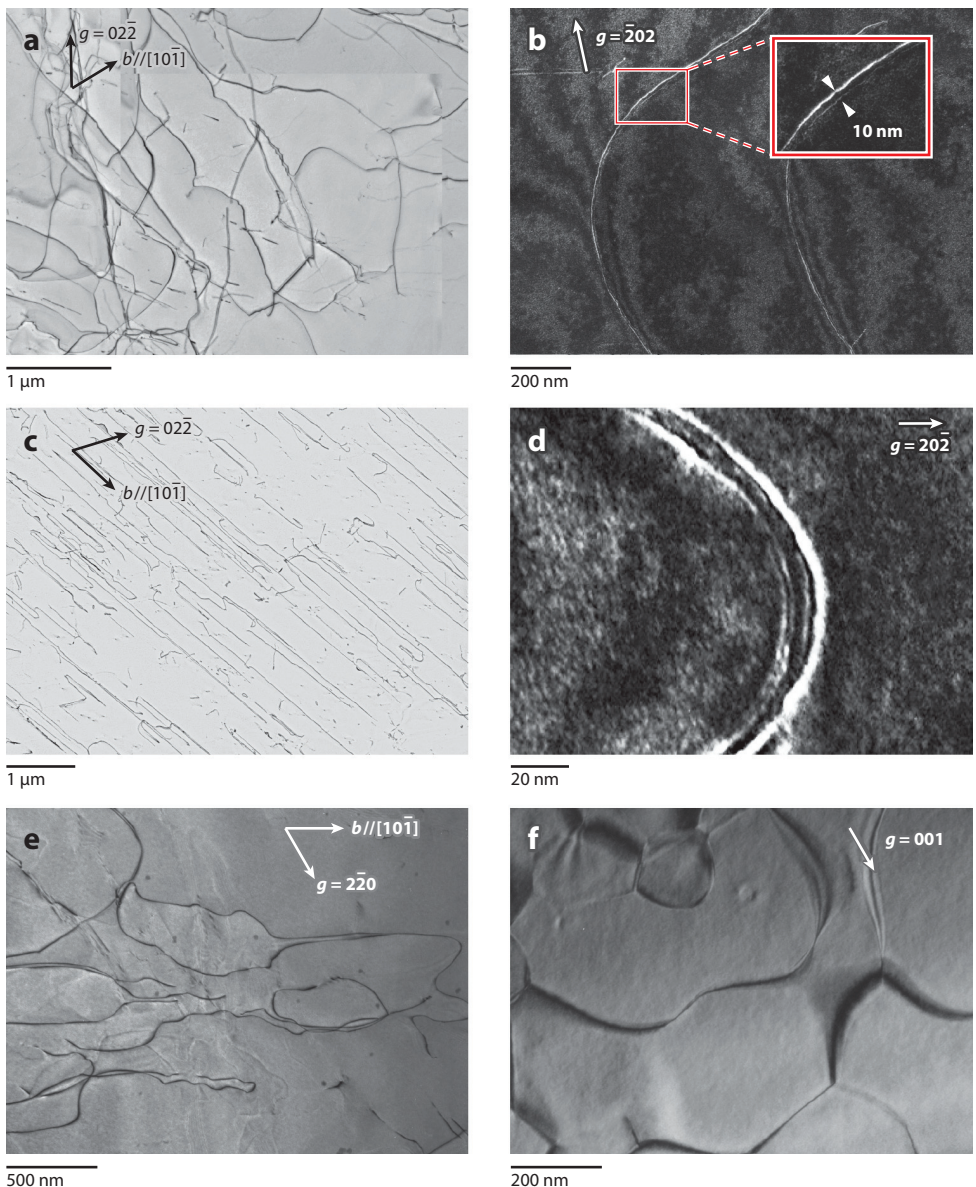


Figure 8

Dislocation structures in Co-12Al-11W alloy polycrystals deformed at (a,b) -196°C , (c,d) 700°C , and (e,f) $1,000^{\circ}\text{C}$. Adapted from Reference 43 with permission.

plane without any preferred orientations (**Figure 8a**), and they dissociate according to the APB scheme (**Figure 8b**) (43). This behavior clearly indicates that the rapid decrease in yield stress observed at low temperatures is ascribed to a thermal component of solid-solution hardening that occurs for the motion of APB-coupled dislocations with a planar and glissile core structure (43). The plateau stress observed in the temperature range from room temperature to 680°C can thus be considered to correspond to the athermal component of solid-solution hardening.

In spite of the considerably high onset temperature for the yield stress anomaly (680°C), the anomaly observed in $\text{Co}_3(\text{Al},\text{W})$ is ascribed to the thermally activated cross-slip of APB-coupled dislocations from (111) to (010), as in the case of many other L1_2 compounds (41, 42), according to the dislocation structure. Dislocations have a strong tendency to align parallel to their screw orientation. Screw segments are locked in the Kear-Wilsdorf configuration, with the APB between coupled partials being on (010), and they are connected to each other by superkinks with edge components (**Figure 8c**). Fourfold dissociation occurs along the superkink (**Figure 8d**). Such dissociation indicates that further subdissociation into Shockley partials with $\mathbf{b} = 1/6\langle 112 \rangle$ occurs for each APB-coupled superpartial dislocation with $\mathbf{b} = 1/2\langle 110 \rangle$, forming a complex stacking fault (CSF) between Shockley partials. The APB and CSF energies are evaluated to be 146 and 137 mJ/m², respectively (43). The CSF energy is very low and is considered to be responsible for the considerably high onset temperature for the yield stress anomaly because the driving forces for cube cross-slip—i.e., the anisotropy in APB energy [the ratio of the APB energy on (111) to that on (001)] and the torque force arising from the elastic anisotropy—are considered to be sufficiently large in $\text{Co}_3(\text{Al},\text{W})$ (43). The high onset temperature of the yield stress anomaly leads to an inferior high-temperature strength of $\text{Co}_3(\text{Al},\text{W})$ in relation to Ni_3Al -base L1_2 compounds that have lower onset temperatures.

In $\text{Co}_3(\text{Al},\text{W})$ with a particular composition of Co-12Al-11W, the yield stress anomaly occurs only in a narrow temperature range from 680°C to 830°C, followed by a rapid decrease at high temperatures. The rapid decrease in yield stress above 830°C is due to (111) slip in the γ phase because the test temperature is above the order-disorder transition temperature. Dislocations are thus curved in places to combine with thermal APBs (**Figure 8e**), which are formed during the reordering that occurs during the cooling after deformation (**Figure 8f**). The occurrence of (111) slip is quite different from what occurs in many other Ni_3Al - and Co_3Ti -base L1_2 compounds in which high-temperature deformation proceeds by slip on (010). In other words, in $\text{Co}_3(\text{Al},\text{W})$, the transformation from the γ' phase to the γ phase occurs before slip on (010), if it occurs, starts to operate at high temperatures. If the stability of the L1_2 phase is improved so as to result in the higher γ' -solvus temperature, the temperature range of the yield stress anomaly is extended toward higher temperatures up to the point at which slip on (001) starts to operate.

As discussed above, a higher γ' -solvus temperature is required for improving the high-temperature strength of the $\gamma'\text{-Co}_3(\text{Al},\text{W})$ phase by extending the temperature range of the yield stress anomaly toward higher temperatures. In addition, a lower onset temperature for the yield stress anomaly is necessary to increase the intermediate- and high-temperature strength of the γ' phase by the yield stress anomaly. The intermediate- and high-temperature strength of $\text{Co}_3(\text{Al},\text{W})$ is substantially lower than that of other L1_2 compounds such as Ni_3Al (41, 48) and Co_3Ti (44, 49), as seen from the normalized plot of yield stress–temperature curves (**Figure 9b**), which is converted from the corresponding yield stress–temperature curves (**Figure 9a**). The high onset temperature for the yield stress anomaly for $\text{Co}_3(\text{Al},\text{W})$ arises principally from the low CSF energy that makes cross-slip of APB-coupled dislocations from (111) to (010) more difficult, because a constriction has to be formed before cross-slip occurs. Increasing the γ' -solvus temperature and the CSF energy of $\text{Co}_3(\text{Al},\text{W})$ also improves the creep strength of Co-base superalloys (50, 51), as discussed in Section 4. Therefore, it is very important to select alloying elements that can simultaneously increase both the γ' -solvus temperature and the CSF energy of $\text{Co}_3(\text{Al},\text{W})$. Alloying elements that increase the γ' -solvus temperature also tend to increase the CSF energy, because both parameters are related to the stability of the $\text{L1}_2\text{-Co}_3(\text{Al},\text{W})$ phase. Additions of Ta, Nb, and Ti as well as large amounts of Ni are expected to be effective, as discussed in Section 2.2. The onset temperature of the yield stress anomaly of a single-phase L1_2 compound, $(\text{Co}_{0.8}\text{Ni}_{0.2})_3(\text{Al},\text{W})$, indeed decreases from 680°C to 430°C.

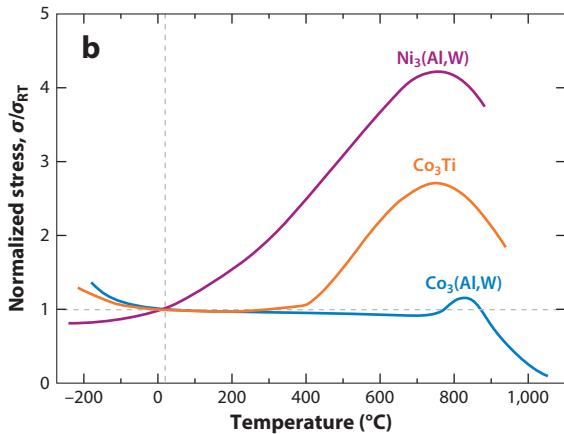
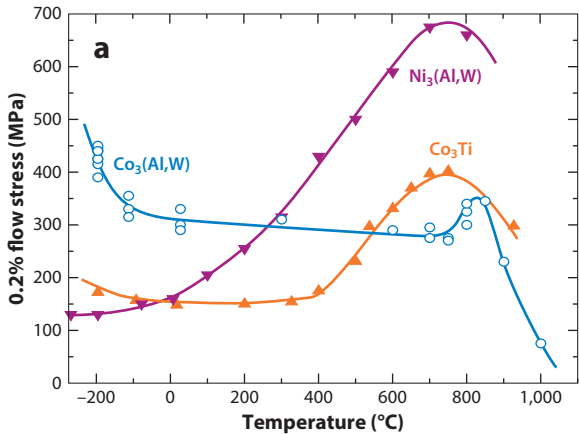


Figure 9

(a) Yield stress–temperature curves of $\text{Co}_3(\text{Al},\text{W})$ (43), Co_3Ti (49), and $\text{Ni}_3(\text{Al},\text{W})$ (48). (b) The normalized plots from these yield stress–temperature curves. The normalization of yield stress was made to that at room temperature for each compound.

4. MECHANICAL BEHAVIOR OF γ' -STRENGTHENED CO-BASE ALLOYS

Figure 10 shows the temperature dependence of the flow stress of ternary Co-Al-W single-crystal and polycrystal alloys as well as Ta- and Ni-containing variants (3; T.M. Pollock, unpublished work). The γ' -containing Co-base alloys are stronger than the solid-solution-strengthened conventional Co-base alloys (such as Haynes188) across the entire temperature range in which the

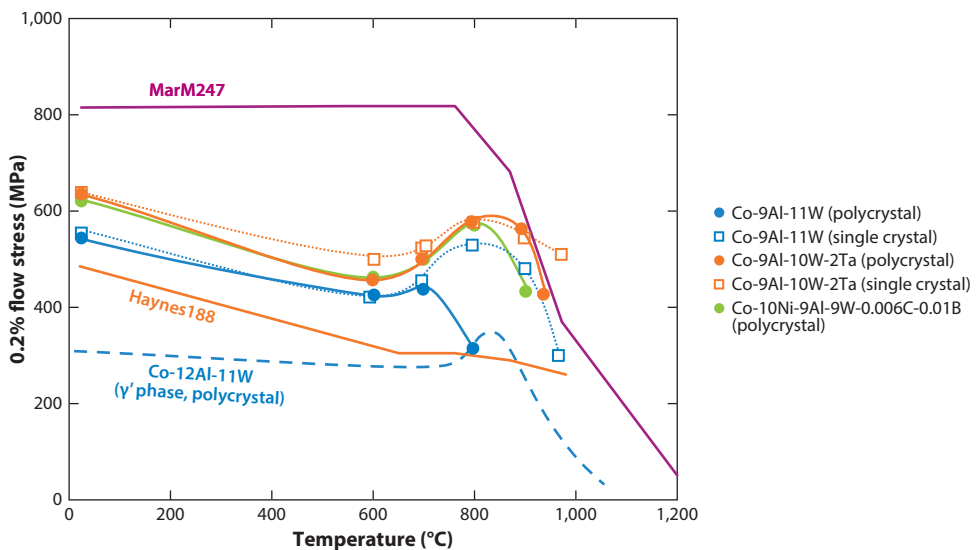


Figure 10

Temperature dependence of the flow stress of polycrystal and single-crystal ternary Co-Al-W alloys and their variants containing Ta and Ni. Co-9Al-11W and Co-9Al-10W-2Ta data are from Reference 3, Co-10Ni-9Al-9W-0.006C-0.01B data are from T.M. Pollock (unpublished work), Co-12Al-11W data are from Reference 43, and MarM247 and Haynes188 data are from Reference 11.

precipitates are thermodynamically stable. The strength of the two-phase alloys also exceeds that of the single-phase γ' -Co₃(Al,W), which arises due to the resistance of the γ' precipitates to shearing by dislocations. The strength of the γ' -containing polycrystals falls short of that of comparable Ni-base superalloys (e.g., MarM247), likely because there is a lower degree of solid-solution strengthening in the γ -Co matrix than in the matrix in Ni-base superalloys, although as discussed further below, another reason may be differences in the shearing resistance of the precipitates in the Co-base alloys. Additions of 2-at% Ta and 10-at% Ni result in improved strength compared with the strength of the ternary alloy.

Similar to the case for single-phase γ' -Co₃(Al,W), the two-phase alloys exhibit an anomalous rise in flow stress above 800°C, with peak flow stresses in excess of 600 MPa. The peak in flow stress is followed by a precipitous drop that is induced by the rapid decay in the volume fraction of precipitates present as a function of temperature, up to complete dissolution of the γ' precipitates, causing a reduction in strength by 3 to 4 times. The Ta-containing single-crystal alloy has the highest strength at 1,000°C, exceeding the strength of Ni-base superalloys at this temperature. This alloy has the highest γ' -solvsus at 1,079°C among the three alloys compared here (3). At temperatures below the peak in flow stress, the primary deformation mechanism is slip on {110}{111} systems. With increasing temperature, {110}{001} slip is thermally activated, and detailed transmission electron microscopy studies have demonstrated cross-slip of 1/2{110} dislocations from the octahedral {111} plane to the cube {001} plane in the precipitates (2), similar to what is observed in γ' single-phase Co-base alloys (Section 3.2) and $\gamma + \gamma'$ two-phase Ni-base alloys (52).

High-temperature creep behavior is of critical importance to the application of this new class of alloys. To date, creep properties have been investigated in both polycrystalline alloys (53–55) and single-crystal alloys (50, 51, 56–58) (**Figures 11 and 12**). Polycrystalline alloys of composition Co-9Al-(8–9)W-2Ta-2X (where X = Nb, Mo, Ir, V, Cr, or Si) show relatively poor creep properties in compression compared with polycrystalline Ni alloys due to extensive damage accumulation at grain boundaries (53). Additions of B improve creep properties, increasing the resistance of grain boundaries to damage accumulation (53, 54). Across the range of compositions investigated in

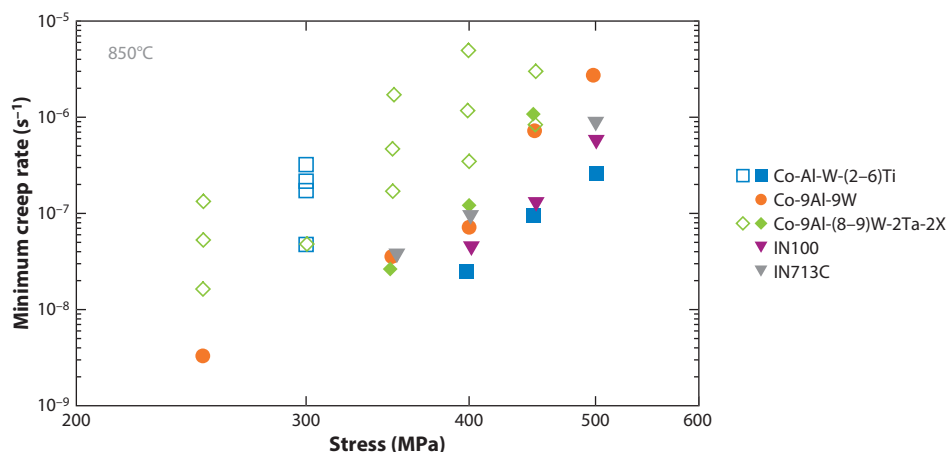


Figure 11

Creep properties of polycrystalline Co-base alloys (53–55) in comparison to creep properties of the commercial polycrystal Ni-base alloys IN100 and IN713C. Filled symbols indicate alloys with B additions, whereas open symbols indicate alloys with no B additions.

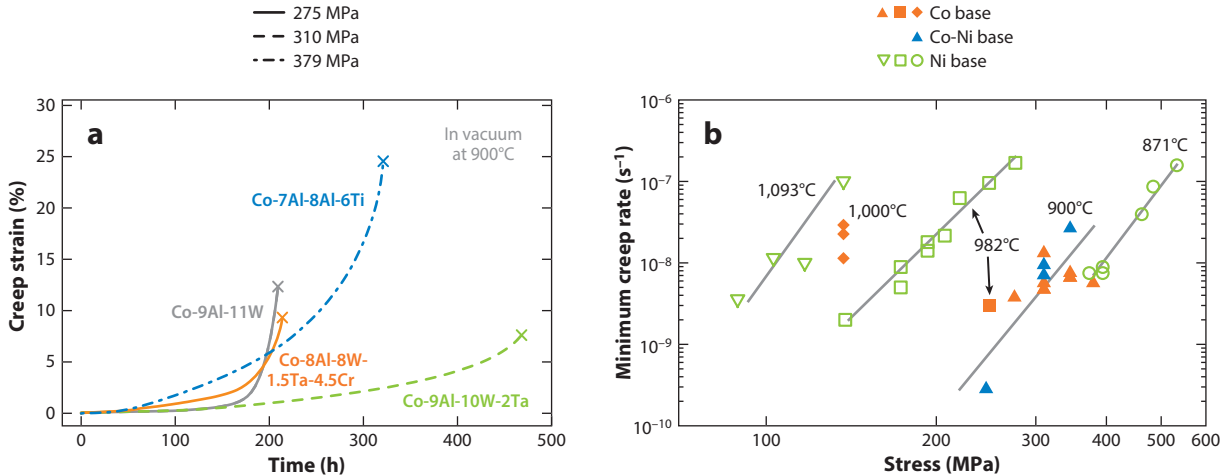


Figure 12

(a) Tension creep curves of Co-Al-W ternary and Ta-, Cr-, and/or Ti-containing alloys at 900°C. Adapted from Reference 57 with permission. (b) Creep properties of single crystals of Co-base and Co-Ni-base alloys (50, 51, 56–58) in comparison to creep properties of Ni-base single crystals of René N4 (52).

Figure 11, intermetallic precipitates were observed at grain boundaries; their role in the creep process is incompletely understood.

Without the complication of grain boundaries, single crystals permit an assessment of creep properties in tension and an examination of the roles of alloying additions. **Figure 12a** shows tension creep curves at 900°C for several different Co-base alloys (57). Primary creep strains are very limited, and creep ductilities are in the range of 5–25%. Creep ductilities are overall somewhat higher in Co-Ni-based alloys, exceeding 25% across a range of compositions (50). **Figure 12b** compares the creep properties of single crystals of Co-base and Co-Ni-base alloys (50, 51, 56–58) in comparison to Ni-base single crystals of René N4 (52). In general, both Co-base and Co-Ni-base alloys show properties comparable to or better than those of first-generation Ni-base single crystals. The alloys with the lowest creep rates across this temperature range are in general Ti- and/or Ta-containing compositions (50, 57, 58). Co-Ni interdiffusion coefficients decrease toward the Co-rich end of the Co-Ni binary system (59), so Co-base alloys are expected to have lower creep rates than would alloys containing some level of Ni addition. However, the unfavorable effect of Ni on the interdiffusion coefficient is offset due to the favorable effect of Ni on the stability of the γ' - $\text{Co}_3(\text{Al},\text{W})$ phase, permitting higher volume fractions of precipitates at elevated temperatures.

An interesting array of deformation mechanisms occur during creep of these new Co-base alloys. In the early stages of creep, deformation occurs predominantly by glide of $a/2\langle 110 \rangle$ dislocations through the γ -Co (fcc) matrix, with a higher initial dislocation content in the vertical channels due to the stress state induced by the positively misfitting precipitates. As with Ni-base superalloys, these Co-base alloys undergo rafting (50, 52, 57, 60), with the important distinction that the rafts generally evolve with their longitudinal axis parallel to the applied tension, due to positive misfit. Alloys with near zero misfit tend to be the weakest in creep (50), and to date the most creep-resistant alloys have been observed to possess negative misfit. Mughrabi (61) suggested that the positive misfit is more beneficial to properties than is negative misfit, due to

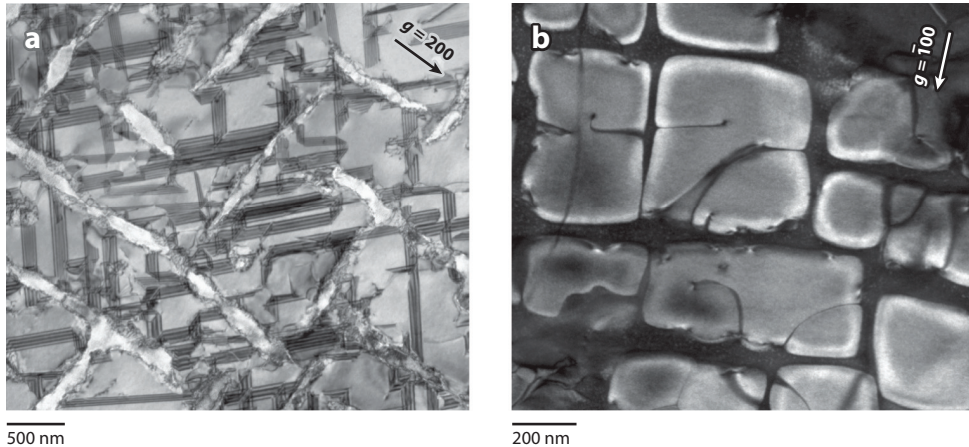


Figure 13

(a) A Co-7Al-8W-6Ti quaternary alloy exhibiting superlattice intrinsic stacking faults and superlattice extrinsic stacking faults following 2% creep at 900°C. (b) Creep-induced antiphase boundaries in precipitates of a Co-29Ni-10Al-6W-6Cr-2Ta alloy. From Reference 62 with permission.

the temperature dependence of the misfit as well as due to the differences in constraint and the associated elastic loading of the precipitates. Isolating the role of misfit is, however, experimentally difficult, given that changes in composition affect many aspects of structure and properties.

At elevated temperatures (up to the γ' -solvsus temperature), extensive shearing of the γ' phase in Co-base alloys has been observed. The shearing process results in the formation of SISFs and SESFs (superlattice extrinsic stacking faults) by a process that involves the reaction of two unit matrix dislocations at the γ - γ' interface that form $a/3\langle 112 \rangle$ super-Shockley partial dislocations that shear the precipitate while leaving a second $a/6\langle 112 \rangle$ partial dislocation at the precipitate-matrix interface (50, 57, 62). After creep deformation at 900°C, high densities of faults are observed in the precipitates (**Figure 13a**). Under similar creep strain conditions in Ni-base alloys, the precipitates are sheared by pairs of APB-coupled $a/2\langle 110 \rangle$ dislocations. Because these dislocation pairs typically glide across the entire diameter of a precipitate, there is little evidence of the contribution of these shearing events to the total creep strain in Ni-base alloys. In this sense, the faults formed in Co-base alloys during creep provide a unique marker of the deformation history. Experimental measurements of the average number of faults per precipitate that develop during creep, along with an analysis of the strain induced by each faulting event, allow for an assessment of the fraction of creep strain that is accumulated by precipitate shearing. In a Co-9Al-10W-2Ta quaternary alloy crept to 0.6%, the shearing process was determined to constitute approximately 20–25% of the total creep strain (63).

In Co-Ni-base alloys, another unusual mode of shearing of the γ' phase becomes prominent as the Ni content increases (62). During high-temperature creep, shearing of precipitates occurs by the motion of unit $a/2\langle 110 \rangle$ dislocations that leave behind APBs in the ordered precipitates (**Figure 13b**). Across the range of compositions from Co-base to Co-Ni-base alloys, the mode of γ' shearing is largely unaffected by the size, volume fraction, and morphology of the γ' precipitates. This finding indicates an important role for both the APB and SISF energies in the γ' phase for mechanical properties.

Using DFT [as implemented in VASP (Vienna Ab Initio Simulation Package)], the axial next-nearest-neighbor Ising model, and special quasi-random structures, Mottura and colleagues

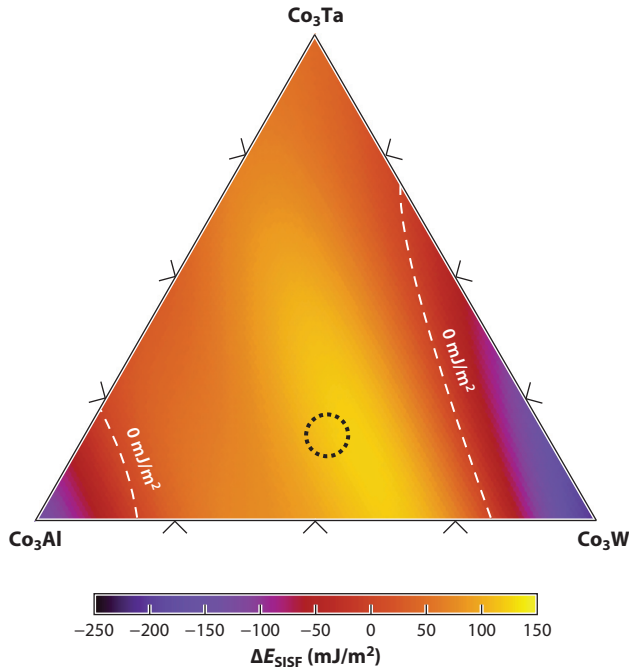


Figure 14

The superlattice intrinsic stacking fault (SISF) energy in the pseudoternary $\text{Co}_3\text{Al}-\text{Co}_3\text{W}-\text{Co}_3\text{Ta}$ system. Contour lines at 0 mJ/m^2 are drawn for clarity (*white dashed lines*). Negative SISF energies correspond to a stabilization of the D_{019} phase. The approximate composition of the precipitates in the $\text{Co}-9\text{Al}-10\text{W}-2\text{Ta}$ alloy is indicated by the black dotted circle.

(24, 25, 63) calculated the SISF energies in ternary and quaternary variants of the γ' (L_{12}) phase. For ternary $\text{Co}_3(\text{Al},\text{W})$ with equal proportions of Al and W, the SISF energy is $89\text{--}93 \text{ mJ/m}^2$, which is approximately a factor of two higher than that of Ni_3Al (64–66). Therefore, a higher stress is required to shear the ordered precipitates in this mode in Co-base materials compared with the case for Ni-base alloys. SISF energies were also calculated for the γ' (L_{12}) phase at compositions across the $\text{Co}-\text{Al}-\text{W}-\text{Ta}$ quaternary system (63); **Figure 14** summarizes the results. These calculations make apparent that the fault energies and the associated resistance to shearing are very sensitive to the composition of the precipitates. For example, **Figure 14** indicates the approximate composition of the precipitates in the $\text{Co}-9\text{Al}-10\text{W}-2\text{Ta}$ alloy. The calculations indicate that the SISF energy is at the high end of the spectrum that could be achieved in the pseudoternary system, consistent with the high creep strength of this composition. It is further apparent that enrichment of Al or W may significantly reduce the fault energy. As more complex variants of these alloys are designed to optimize a broader set of properties, it will be important to tailor the compositions of the precipitates to ensure high SISF energies. DFT studies again provide useful guidance in this context. In calculations that address the difference in energy between Co_3X (where X = a transition metal) in the form of the L_{12} structure and Co_3X in the D_{019} crystal structure [the differences in energy directly yield the SISF energy (25)], elements most likely to stabilize the L_{12} structure and to increase the SISF energy include Ta, Ti, Nb, V, and Hf (**Figure 15**).

With regard to APB energies, Vamsi and colleagues (67, 68) calculated planar defect energies for ternary stoichiometric and binary and ternary off-stoichiometric compositions of $\text{Co}_3\text{W}_{1-x}\text{Al}_x$ in comparison to $\text{Ni}_3\text{Al}_{1-x}\text{Ti}_x$ by using DFT. At $x = 0.5$, $\text{Co}_3(\text{W},\text{Al})$ has a lower APB energy

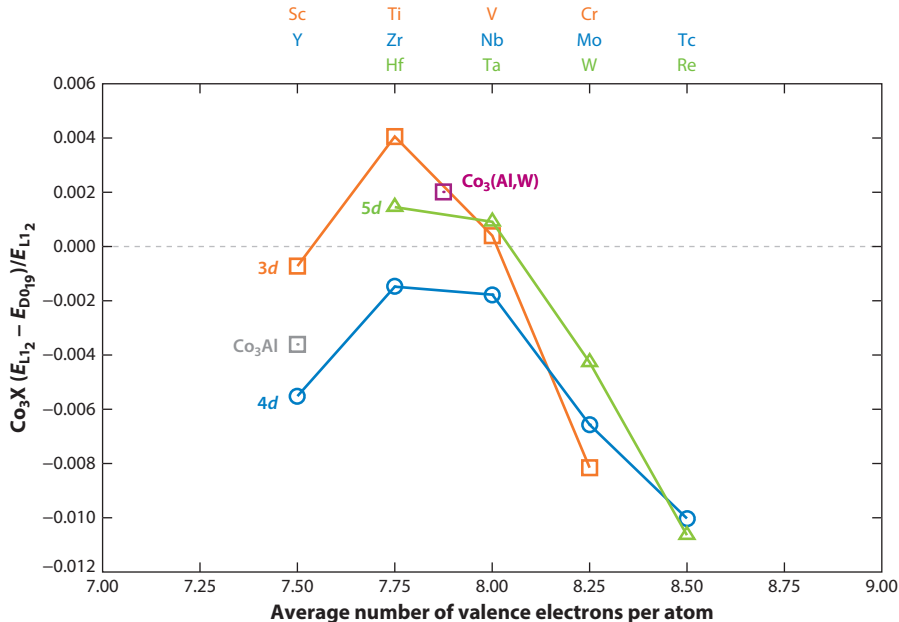


Figure 15

The relative energies of $\text{L1}_2\text{-Co}_3\text{X}$ and $\text{D}0_{19}\text{-Co}_3\text{X}$, where X is Sc, Ti, V, Cr, Y, Zr, Nb, Mo, Tc, Hf, Ta, W, or Re, plotted against the average number of valence electrons per atom. Adapted from Reference 25 with permission.

(approximately 300 mJ/m²) than does $\text{Ni}_3(\text{Al,Ti})$ (approximately 475 mJ/m²). Thus, for ternary Co-Al-W compositions, the SISF energy is significantly lower than the APB energy, consistent with the appearance of SISF faults during creep deformation. Interestingly, as both $\text{Co}_3(\text{W,Al})$ and $\text{Ni}_3(\text{Al,Ti})$ become rich in Al, the APB energies fall substantially. Further studies in which Ni is substituted on the Co lattice in $\text{Co}_3(\text{W,Al})$ would clearly be useful. However, on the basis of the fact that Co-base alloys form SISFs during creep deformation whereas Co-Ni alloys form APBs, the substitution for Ni on the Co lattice in $\text{Co}_3(\text{W,Al})$ is likely to reduce the APB energy and/or increase the SISF energy. Again, further detailed studies are needed to understand the trends in multicomponent space.

Whereas the SISF and APB energies of the precipitates clearly influence creep as well as higher rate flow properties of these alloys, how they influence fatigue properties is not clear. In Ni-base alloys, low-cycle fatigue and high-cycle fatigue involve deformation with intense planar slip, whereby precipitates are sheared extensively with a high level of slip irreversibility (69–72). Given the possibility of higher fault energies, the resistance to fatigue may be higher in Co-base systems than in Ni-base systems; experiments on fatigue properties across a range of temperatures and stresses are clearly required.

5. OXIDATION BEHAVIOR

There have been limited studies on oxidation behavior of Co-Al-W-base alloys (12, 73–78). Formation of a protective dense oxide layer consisting of either Cr_2O_3 or Al_2O_3 , depending on the target application temperature, is required in high-temperature applications. **Figure 16** shows a

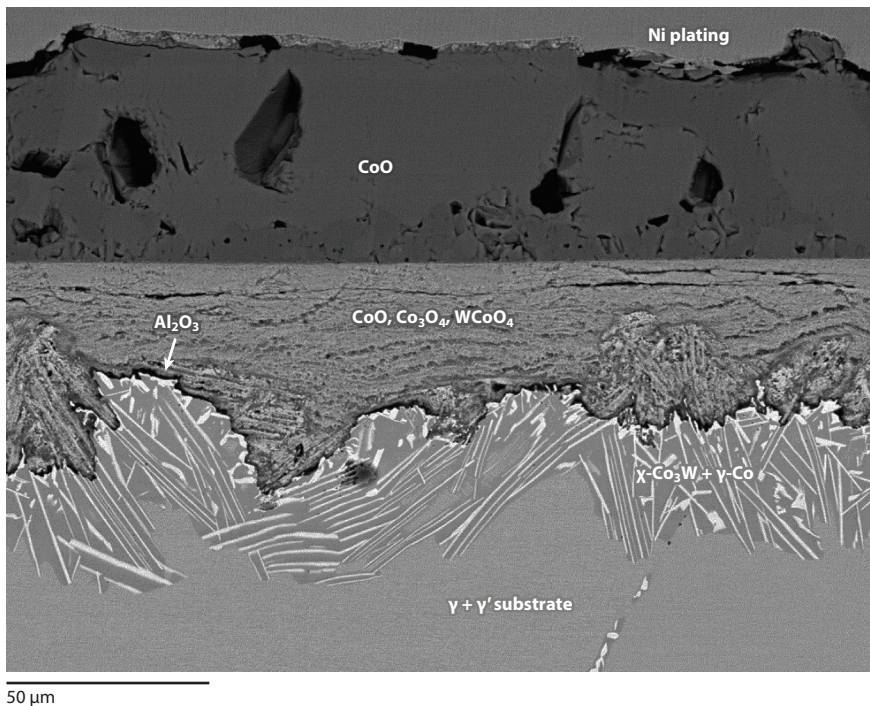


Figure 16

A backscattered electron micrograph of the surface oxide layer formed on a Co-8Al-8W-4.5Cr-1.5Ta alloy after exposure in air at 900°C for 168 h. Adapted from Reference 12 with permission.

typical oxide structure formed at 900°C on a Co-Al-W-base alloy containing Cr and Ta (12). The outer layer consists of thick, porous CoO, and the inner layer consists of a complex mixture of CoO, Co₃O₄, and a W-rich oxide such as WC_oO₄. Depending on alloy compositions, a very thin layer of Al₂O₃ is formed at the oxide-metal interface. In the substrate, due to the outward elemental diffusion to form the oxides, an interdiffusion zone consisting of γ -Co and D_{0.9} forms. Yan et al. (73) conducted semicyclic oxidation tests by using ternary and quaternary alloys at 800°C. All alloys exhibited parabolic oxide growth behavior. After exposure for 196 h, the alloys with Cr, Fe, Si, or Ta showed smaller weight gains than did the ternary alloy, and higher weight gains were observed with additions of Ni, Ti, Mo, and V. **Figure 17** shows comparisons of alloying elements with regard to weight gain. Si and Ta are the most effective elements on a per-atomic-percent basis, although the solubility of these elements is limited. Cr and Fe can be added by large amounts, and Cr is more effective than Fe. The effect of Ni is negligible, and the additions of Mo and V have detrimental effects. The alloy with 10% Cr forms thin oxide layers consisting of a spinel Al₂CoO₄ (the outer layer) and CrO₂, Cr₂O₃, and Al₂O₃ (the inner layer), whereas other Cr-free alloys form thick oxide layers consisting of Co₃O₄ (the outer layer) and Co₃O₄ and Al₂O₃ (the inner layer). Klein et al. (74) investigated the effect of additions of B and observed reduced weight gain with increased B content up to 0.12% at 800°C and 900°C. Boride formation in the inner oxide layer is considered to improve oxide adhesion. Addition of Si was also beneficial above 900°C by promoting alumina formation (75). There are very limited studies at temperatures greater than 1,000°C, beyond which an Al₂O₃ protective layer is required (76). A comparison of alloys containing 10% and 20% Ni showed that additions of greater amounts of Ni have a positive

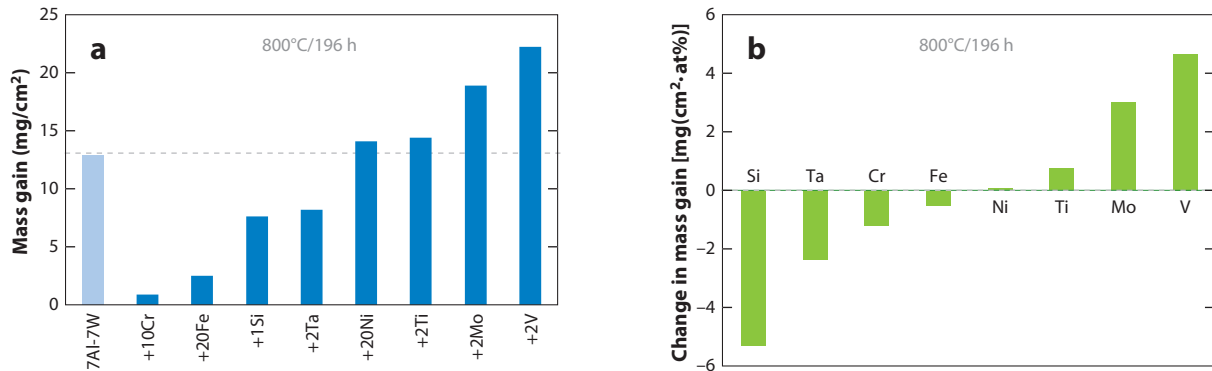


Figure 17

- (a) Mass gains of a Co-7Al-7W ternary alloy and various quaternary alloys after semicyclic oxidation at 800°C for 196-h exposures.
(b) Changes in mass gain per 1-at% addition of quaternary alloying elements. Original data from Reference 73.

effect in delaying oxide spallation during cyclic oxidation. However, a protective oxide layer does not form. To improve oxidation resistance, further research is required to understand the effects of impurities; of minor elements, such as rare earth elements, B, C, and Si; and of combined additions of beneficial elements, such as Cr, Al, Ni, and Ta. For higher-temperature applications, the development of compatible coatings will also be required (12, 76, 79). Preliminary investigations of CoNiCrAlY coatings applied to a ternary Co-Al-W alloy and an alloy containing Cr and Ta demonstrated good alloy-coating compatibility (79).

6. OUTLOOK

Conventional Co alloys such as Haynes188, L605, and FSX414 currently find applications in industrial gas turbines, aircraft engines, and biomedical implants. Thus, the availability of higher-strength- and/or higher-temperature-capable Co-base alloys is likely to be of interest in many of these same applications as new designs are developed, particularly in aircraft engines and industrial turbines with higher turbine inlet temperatures. In turbine engines, nonrotating components such as vanes and elements of the combustor system represent lower risk for introduction compared with turbine blades or turbine disks. As with Ni-base superalloys, the compositions that are ultimately developed as engineering materials that serve in these different applications are likely to be significantly different from the simple compositions reported here. For example, if a new Co-base alloy were developed for a turbine blade application, it would likely be employed in single-crystal form. Therefore, the major design criteria would center on higher solvus temperatures, high creep and fatigue resistance, good oxidation resistance, compatibility with thermal barrier coatings, and a low tendency for convective instabilities during directional solidification. As mentioned in Section 4, DFT calculations provide directions for the design of more complex multicomponent alloys with a balance of mechanical properties. Compositional domains that might be favorable for oxidation and corrosion are much less understood, but a highly desirable trait would be formation of protective α -Al₂O₃ during intermediate- and high-temperature exposures. Recent single-crystal solidification studies (80) demonstrate very interesting trends. The dendritic segregation that occurs in alloys examined to date demonstrates a low degree of segregation of Al, W, Co, and Cr, with Scheil partition coefficients between 0.93 and 1.01. Ta segregates preferentially to the liquid during solidification, with $k = 0.53\text{--}0.63$, which would stabilize against convective instabilities

during solidification. To date, none of the compositions examined experimentally have shown any propensity for the formation of freckles. Freckle defects are small chains of equiaxed grains formed by the fragmentation of dendrite arms during solidification, which is caused by convective instabilities in the mushy zone that develop as a result of density inversions created by progressive segregation of individual alloying elements (6). Because freckle defects consist of misoriented grains, they are detrimental to the mechanical properties of single-crystal alloys. This favorable partitioning of solute during solidification in Co-base alloy systems is in contrast to the case for Ni-base single crystals, which display strong tendencies for convective instabilities, particularly in alloys containing high levels of Re and W (81, 82). For this reason, this new class of new Co-base alloys may be particularly attractive for application in large, complex single-crystal or directionally solidified castings in which freckling and the formation of misoriented grains are major challenges. Co-base superalloys may also be suitable for a cast-and-wrought processing route for turbine disks and sheet component applications. Regarding such superalloys, their relatively narrow freezing ranges between the liquidus and solidus temperatures (12, 30, 31) are favorable for producing large-diameter ingots without severe segregation. Their relatively large windows between the solidus and γ' -solvus temperatures (30, 31) are also beneficial for hot working, such as forging, extruding, and hot rolling. McDevitt (83) recently demonstrated that an ingot metallurgy route for producing a 22-kg cast-and-wrought Co-9Al-9W-2Ti-0.02B alloy was feasible using conventional vacuum induction melting, vacuum arc remelting, and forging. Further studies on solidification and thermomechanical processing as well as on welding, joining, forming, and machining will be required to establish the processing and manufacturing routes for Co-base superalloys.

7. SUMMARY

The current understanding of γ' -Co₃(Al,W) phase and γ' -strengthened Co-base superalloys and Ni-base alloys is reviewed above. Relatively low stacking fault energies and low stability of the γ' phase compared with the γ' phase in Ni-base alloys are responsible for the unique deformation behaviors observed in γ' single-phase and $\gamma + \gamma'$ two-phase alloys. Further alloy studies with a guidance of computational modeling capability is critical for controlling energies of planar defects, such as stacking faults and APBs, by alloying additions. Experimental and DFT studies indicate that additions of Ta, Ti, Nb, Hf, and Ni are effective in simultaneously increasing both the phase stability and stacking fault energy of γ' -Co₃(Al,W), thus improving the high-temperature strength of Co-base γ' phase and $\gamma + \gamma'$ two-phase superalloys by enhancing the flow stress anomalies and the shear resistance of the γ' phase.

DISCLOSURE STATEMENT

The authors are not aware of any affiliations, memberships, funding, or financial holdings that might be perceived as affecting the objectivity of this review.

ACKNOWLEDGMENTS

T.M.P. is grateful for the contributions of M. Titus, R. Rhein, and A. Van der Ven to this manuscript. The support of General Electric and NSF DMREF grant DMR 1233704 is also acknowledged (A.S. and T.M.P.). H.I. greatly appreciates the support of JSPS KAKENHI (24246113 and 25630304); the Elements Strategy Initiative for Structural Materials from the Ministry of Education, Culture, Sports, Science and Technology of Japan; and the Advanced Low Carbon Technology Research and Development Program from the Japan Science and Technology Agency.

LITERATURE CITED

1. Sato J, Omori T, Oikawa K, Kainuma R, Ishida K. 2006. Cobalt-base high temperature alloys. *Science* 312:90–91
2. Suzuki A, DeNolf GC, Pollock TM. 2007. Flow stress anomalies in γ/γ' two-phase Co-Al-W-base alloys. *Scr. Mater.* 56:385–88
3. Suzuki A, Pollock TM. 2008. High-temperature strength and deformation of γ/γ' two-phase Co-Al-W-base alloys. *Acta Mater.* 56:1288–97
4. Sims CT, Stoloff NS, Hagel WC. 1987. *Superalloys II*. New York: Wiley
5. Reed RC. 2008. *The Superalloys, Fundamentals and Applications*. Cambridge, UK: Cambridge Univ. Press
6. Pollock TM, Tin S. 2006. Nickel-based superalloys for advanced turbine engines: chemistry, microstructure, and properties. *J. Propul. Power* 22:361–74
7. Beltran AM. 1987. Cobalt-base alloys. See Ref. 4, pp. 135–63
8. Sullivan CP, Donachie MJ Jr, Morral FR. 1970. *Cobalt-Base Superalloys—1970*. Brussels: Cent. Inf. Cobalt
9. Tien JK. 1972. On the celestial limit of nickel-base superalloys. In *Proc. Superalloys 2012*, pp. W1–16. Columbus, OH: Met. Ceram. Inf. Cent.
10. Huron ES, Reed RC, Hardy MC, Mills MJ, Montero RE, et al., ed. 2012. *Superalloys 2012*. Hoboken, NJ: Wiley
11. Gabb TP, Dreshfield RL. 1987. Superalloy data. In *Superalloys II*, ed. CT Sims, NS Stoloff, WC Hagel, pp. 575–97. New York: Wiley
12. Pollock TM, Dibbern J, Tsunekane M, Zhu J, Suzuki A. 2010. New Co-based $\gamma-\gamma'$ high-temperature alloys. *JOM* 62:58–63
13. Encinas-Oropesa A, Drew GL, Hardy MC, Leggett AJ, Nicholls JR, Simms NJ. 2008. Effects of oxidation and hot corrosion in a nickel disc alloy. In *Proc. Superalloys 2008*, pp. 609–18. Warrendale, PA: Miner. Met. Mater. Soc.
14. Gabb TP, Telesman J, Kantzios PT, Smith JW, Browning PF. 2004. Effects of high temperature exposures on fatigue life of disk superalloys. In *Proc. Superalloys 2004*, pp. 269–74. Warrendale, PA: Miner. Met. Mater. Soc.
15. Guédou JY, Augustins-Lecallier I, Nazé L, Caron P, Locq D. 2008. Development of a new fatigue and creep resistant pm nickel-base superalloy for disk applications. In *Proc. Superalloys 2008*, pp. 21–30. Warrendale, PA: Miner. Met. Mater. Soc.
16. Kobayashi S, Tsukamoto Y, Takasugi T, Chinen H, Omori T, et al. 2009. Determination of phase equilibria in the Co-rich Co-Al-W ternary system with a diffusion-couple technique. *Intermetallics* 17:1085–89
17. Omori T, Oikawa K, Sato J, Ohnuma I, Kattner UR, et al. 2013. Partition behavior of alloying elements and phase transformation temperatures in Co-Al-W-base quaternary systems. *Intermetallics* 32:274–83
18. Lass E, Williams ME, Campbell CE, Moon K-W, Kattner UR. 2014. γ' phase stability and phase equilibrium in ternary Co-Al-W at 900°C. *J. Phase Equilb. Diffus.* 35:711–23
19. Lass E. 2014. *Phase equilibria in the ternary Co-W-Al alloy system*. Presented at TMS Annu. Meet., 143rd, San Diego, CA
20. Jiang C. 2008. First-principles study of $\text{Co}_3(\text{Al},\text{W})$ alloys using special quasi-random structures. *Scr. Mater.* 59:1075–78
21. Saal JE, Wolverton C. 2013. Thermodynamic stability of Co-Al-W L1_2 γ' . *Acta Mater.* 61:2330–38
22. Rhein R, Dodge P, Pollock TM, Van der Ven A. 2014. The stability of the L1_2 phase in the $\text{Co}_3(\text{Al},\text{W})$ system. *Acta Mater.* Submitted
23. Moroni EG, Kresse G, Hafner J, Furthmüller J. 1997. Ultrasoft pseudopotentials applied to magnetic Fe, Co, and Ni: from atoms to solids. *Phys. Rev. B* 56:15629
24. Mottura A, Janotti A, Pollock TM. 2012. A first principles study of the effect of Ta on the superlattice intrinsic stacking fault energy in $\text{L1}_2\text{-Co}_3(\text{Al},\text{W})$. *Intermetallics* 28:138–43
25. Mottura A, Janotti A, Pollock TM. 2012. Alloying effects in the γ' phase of Co-based superalloys. In *Proc. Superalloys 2012*, pp. 685–93. Hoboken, NJ: Wiley
26. Kobayashi S, Tsukamoto Y, Takasugi T. 2011. Phase equilibria in the Co-rich Co-Al-W-Ti quaternary system. *Intermetallics* 19:1908–12

27. Kobayashi S, Tsukamoto Y, Takasugi T. 2012. The effects of alloying elements (Ta, Hf) on the thermodynamic stability of γ' -Co₃(Al,W) phase. *Intermetallics* 31:94–98
28. Ooshima M, Tanaka K, Okamoto NL, Kishida K, Inui H. 2010. Effects of quaternary alloying elements on the γ' solvus temperature of Co-Al-W based alloys with fcc/L1₂ two-phase microstructures. *J. Alloys Compd.* 508:71–78
29. Xue F, Wang M, Feng Q. 2012. Alloying effects on heat-treated microstructure in Co-Al-W-base superalloys at 1300°C and 900°C. In *Proc. Superalloys 2012*, pp. 813–21. Hoboken, NJ: Wiley
30. Bauer A, Neumeier S, Pyczak F, Göken M. 2010. Microstructure and creep strength of different γ/γ' -strengthened Co-base superalloy variants. *Scr. Mater.* 63:1197–200
31. Bauer A, Neumeier S, Pyczak F, Göken M. 2012. Creep strength and microstructure of polycrystalline γ' strengthened cobalt-base superalloys. In *Proc. Superalloys 2012*, pp. 695–703. Hoboken, NJ: Wiley
32. Shinagawa K, Omori T, Sato J, Oikawa K, Ohnuma I, et al. 2008. Phase equilibria and microstructure on γ' phase in Co-Ni-Al-W system. *Mater. Trans.* 49:1474–79
33. Yan HY, Vorontsov VA, Dye D. 2014. Alloying effects in polycrystalline γ' strengthened Co-Al-W base alloys. *Intermetallics* 48:44–53
34. Zhu J, Titus MS, Pollock TM. 2014. Experimental investigation and thermodynamic modeling of the Co-rich region in the Co-Al-Ni-W quaternary system. *J. Phase Equilib. Diffus.* 35:595–611
35. Tanaka K, Ohashi T, Kishida K, Inui H. 2007. Single-crystal elastic constants of Co₃(Al,W) with the L1₂ structure. *Appl. Phys. Lett.* 91:181907
36. Yao Q, Xing H, Sun J. 2006. Structural stability and elastic property of the L1₂ ordered Co₃(Al,W) precipitate. *Appl. Phys. Lett.* 89:161906
37. Wang YJ, Wang CY. 2009. Comparison of the ideal strength between L1₂ Co₃(Al,W) and Ni₃Al under tension and shear from first-principles calculations. *Appl. Phys. Lett.* 94:261909
38. Pettifor DG. 1992. Theoretical predictions of structure and related properties of intermetallics. *Mater. Sci. Technol.* 8:345–49
39. Pugh SF. 1954. Relations between the elastic moduli and the plastic properties of polycrystalline pure metals. *Philos. Mag.* 45:823–43
40. Inui H, Oohashi T, Okamoto NL, Kishida K, Tanaka K. 2011. Mechanical properties of the ternary L1₂ compound Co₃(Al,W) in single and polycrystalline forms. *Key Eng. Mater.* 465:9–14
41. Liu CT, Pope DP. 1995. Ni₃Al and its alloys. In *Intermetallic Compounds Principles and Practice*, Vol. 2, ed. JH Westbrook, RL Fleischer, pp. 17–51. Chichester, UK: John Wiley & Sons
42. Yamaguchi M, Umakoshi Y. 1990. The deformation behaviour of intermetallic superlattice compounds. *Prog. Mater. Sci.* 34:1–148
43. Okamoto NL, Oohashi T, Adachi H, Kishida K, Inui H, Veyssiére P. 2011. Plastic deformation of polycrystals of Co₃(Al,W) with the L1₂ structure. *Philos. Mag.* 91:3667–84
44. Takasugi T, Hirakawa S, Izumi O, Ono S, Watanabe S. 1987. Plastic flow of Co₃Ti single crystals. *Acta Metall.* 35:2015–26
45. Miura S, Ohkubo K, Mohri T. 2007. Mechanical properties of Co-based L1₂ intermetallic compound Co₃(Al,W). *Mater. Trans.* 48:2403–8
46. Wee DM, Pope DP, Vitek V. 1984. Plastic flow of Pt₃Al single crystals. *Acta Metall.* 32:829–36
47. Vitek V, Paidar V. 2008. Non-planar dislocation cores: a ubiquitous phenomenon affecting mechanical properties of crystalline materials. In *Dislocations in Solids*, Vol. 14, ed. JP Hirth, pp. 439–514. Amsterdam: Elsevier
48. Mulford RA, Pope DP. 1973. The yield stress of Ni₃(Al,W). *Acta Metall.* 21:1375–80
49. Oya-Semiyama Y, Shinoda T, Suzuki T. 1996. Low-temperature strength anomaly of L1₂ type intermetallic compounds Co₃Ti and Pt₃Al. *Mater. Trans.* 37:1464–70
50. Titus MS, Suzuki A, Pollock TM. 2012. Creep and directional coarsening in single crystals of new $\gamma-\gamma'$ cobalt-base alloys. *Scr. Mater.* 66:574–77
51. Tanaka K, Ooshima M, Tsuno N, Sato A, Inui H. 2012. Creep deformation of single crystals of new Co-Al-W based alloys with fcc/L1₂ two-phase microstructures. *Philos. Mag.* 92:1–17
52. Pollock TM, Field RD. 2002. Dislocations and high temperature plastic deformation of superalloy single crystals. In *Dislocations in Solids*, Vol. 11, ed. FRN Nabarro, MS Duesbery, pp. 547–618. Amsterdam: Elsevier

53. Bauer A, Neumeier S, Pyczak F, Singer R, Göken M. 2012. Creep properties of different γ' -strengthened Co-base superalloys. *Mater. Sci. Eng. A* 550:333–241
54. Bauer A, Neumeier S, Pyczak D, Göken M. 2014. Influence of iridium on the properties of γ' strengthened Co-base superalloys. *Adv. Eng. Mater.* In press; doi: 10.1002/adem.201400266
55. Zenk CH, Neumeier S, Stone HJ, Göken M. 2014. Mechanical properties and lattice misfit of γ/γ' strengthened Co-base superalloys in the Co-W-Al-Ti quaternary system. *Intermetallics* 55:28–39
56. Pyczak F, Bauer A, Göken M, Neumeier S, Lorenz U, et al. 2013. Plastic deformation mechanisms in a crept L1₂ hardened Co-base superalloy. *Mater. Sci. Eng. A* 571:13–18
57. Titus MS, Suzuki A, Pollock TM. 2012. High temperature creep of new L1₂-containing cobalt-base superalloys. In *Proc. Superalloys 2012*, pp. 823–32. Hoboken, NJ: Wiley
58. Xue F, Zhou H, Chen X, Shi Q, Chang H, et al. 2014. Creep behavior of a novel Co-Al-W-base single crystal alloy containing Ta and Ti at 982°C. *MATEC Web Conf.* 14:15002
59. Cui Y-W, Jiang M, Ohnuma I, Kainuma R, Ishida K. 2008. Computational study of atomic mobility for fcc phase of Co-Fe and Co-Ni binaries. *J. Phase Equilib. Diffus.* 29:1–10
60. Paris O, Fahrmann M, Fahrmann W, Pollock TM, Fratzl P. 1997. Early stages of precipitate rafting in a single crystal Ni-Al-Mo model alloy investigated by small angle X-ray scattering and TEM. *Acta Mater.* 45:1085–97
61. Mughrabi H. 2014. The importance of sign and magnitude of γ/γ' lattice misfit in superalloys—with special reference to the new γ' -hardened cobalt-base superalloys. *Acta Mater.* 81:21–29
62. Titus MS, Eggeler YM, Suzuki A, Pollock TM. 2014. Creep-induced planar defects in L1₂-containing Co- and CoNi-base single crystal superalloys. *Acta Mater.* 77:352–59
63. Titus MS, Mottura A, Viswanathan GB, Suzuki A, Mills MJ, Pollock TM. 2015. High resolution energy dispersive spectroscopy mapping of planar defects in L1₂-containing Co-base superalloys. *Acta Mater.* 89:423–37
64. Fu CL, Yoo MH. 1988. All-electron total-energy theory of crystal elasticity—L1₂-ordered alloys. *Philos. Mag. Lett.* 58:199–204
65. Rosengaard NM, Skriver HL. 1994. Ab initio study of antiphase boundaries and stacking faults in L1₂ and D0₂₂ compounds. *Phys. Rev. B* 50:4848–58
66. Schoeck G, Kohlhammer S, Fahnele M. 1999. Planar dissociations and recombination energy of [110] superdislocations in Ni₃Al: generalized Peierls model in combination with ab initio electron theory. *Philos. Mag. Lett.* 79:849–57
67. Srimannarayana P, Vamsi KV, Karthikeyan S. 2014. Multi-scale modelling of Suzuki segregation in γ' precipitates in Ni and Co-base superalloys. *MATEC Web Conf.* 14:15003
68. Vamsi KV, Karthikeyan S. 2012. Effect of off-stoichiometry and ternary additions on planar fault energies in Ni₃Al. In *Proc. Superalloys 2012*, pp. 521–30. Hoboken, NJ: Wiley
69. Pineau A, Antolovich SD. 2009. High temperature fatigue of nickel-base superalloys—a review with special emphasis on deformation modes and oxidation. *Eng. Fail. Anal.* 16:2668–97
70. Li P, Li QQ, Jin T, Zhou YZ, Li JG, et al. 2014. Comparison of low-cycle fatigue behaviors between two nickel-based single-crystal superalloys. *Int. J. Fatigue* 63:137–44
71. Milligan WW, Antolovich SD. 1987. Yielding and deformation behavior of the single crystal superalloy PWA 1480. *Metall. Mater. Trans. A* 18:85–95
72. Yi JZ, Torbet CJ, Feng Q, Pollock TM, Jones JW. 2007. Ultrasonic fatigue of a single crystal superalloy at 1000°C. *Mater. Sci. Eng. A* 443:142–49
73. Yan HY, Vorontsov VA, Dye D. 2014. Effect of alloying on the oxidation behavior of Co-Al-W superalloys. *Corros. Sci.* 83:382–95
74. Klein L, Shen Y, Killian MS, Virtanen S. 2011. Effect of B and Cr on the high temperature oxidation behavior of novel γ/γ' -strengthened Co-base superalloys. *Corros. Sci.* 53:2713–20
75. Klein L, Killian MS, Virtanen S. 2013. The effect of nickel and silicon addition on some oxidation properties of novel Co-based high temperature alloys. *Corros. Sci.* 69:43–49
76. Adharapurapu A, Perez-Bergquist S, Dibbern J, Suzuki A, Pollock T. 2011. *Cyclic oxidation of Co-Al-W-based alloys*. Presented at TMS Annu. Meet., 140th, San Diego, CA
77. Klein L, Bauer A, Neumeier S, Göken M, Virtanen S. 2011. High temperature oxidation of γ/γ' -strengthened Co-base superalloys. *Corros. Sci.* 53:2027–34

78. Klein L, Zendegani A, Palumbo M, Fries SG, Virtanen S. 2014. First approach for thermodynamic modelling of the high temperature oxidation behaviour of ternary γ' -strengthened Co-Al-W superalloys. *Corros. Sci.* 89:1–5
79. Vermaak N, Mottura A, Pollock TM. 2013. Cyclic oxidation of high temperature coatings on new γ' strengthened cobalt-based alloys. *Corros. Sci.* 75:300–8
80. Tsunekane M, Suzuki A, Pollock TM. 2011. Single-crystal solidification of new Co-Al-W-base alloys. *Intermetallics* 19:636–43
81. Tin S, Pollock TM. 2003. Stabilization of thermosolutal convective instabilities in Ni-based single-crystal superalloys: carbide precipitation and Rayleigh numbers. *Metall. Mater. Trans. A* 34:1953–67
82. Tin S, Pollock TM, Murphy W. 2001. Stabilization of thermosolutal convective instabilities in Ni-based single crystal superalloys: carbon additions and freckle formation. *Metall. Mater. Trans. A* 32:1743–53
83. McDevitt E. 2014. Vacuum induction melting and vacuum arc remelting of Co-Al-W-X γ' superalloys. *MATEC Web Conf.* 14:02001

Contents

2D Materials Beyond Graphene (Venkatraman Gopalan and Bettina Lotsch, Guest Editors)

- Beyond Graphene: Progress in Novel Two-Dimensional Materials
and van der Waals Solids
*Saptarshi Das, Joshua A. Robinson, Madan Dubey, Humberto Terrones,
and Mauricio Terrones* 1

- Inorganic Graphene Analogs
C.N.R. Rao and Urmimala Maitra 29

- Materials for Flexible, Stretchable Electronics: Graphene
and 2D Materials
Sang Jin Kim, Kyoungjun Choi, Bora Lee, Yuna Kim, and Byung Hee Hong 63

- Vertical 2D Heterostructures
Bettina V. Lotsch 85

- Organization of Artificial Superlattices Utilizing Nanosheets as a
Building Block and Exploration of Their Advanced Functions
Renzhi Ma and Takayoshi Sasaki 111

- Tunable Exfoliation of Synthetic Clays
Matthias Stöter, Sabine Rosenfeldt, and Josef Breu 129

Materials Informatics (Richard LeSar and Ram Seshadri, Guest Editors)

- Materials Informatics: The Materials “Gene” and Big Data
Krishna Rajan 153

- Materials Data Science: Current Status and Future Outlook
Surya R. Kalidindi and Marc De Graef 171

- What Is High-Throughput Virtual Screening? A Perspective
from Organic Materials Discovery
*Edward O. Pyzer-Knapp, Changwon Suh, Rafael Gómez-Bombarelli,
Jorge Aguilera-Iparraguirre, and Alán Aspuru-Guzik* 195

Symmetry-Based Computational Tools for Magnetic Crystallography <i>J.M. Perez-Mato, S.V. Gallego, E.S. Tasci, L. Elcoro, G. de la Flor, and M.I. Aroyo</i>	217
---	-----

Current Interest

BiFeO ₃ Thin Films: A Playground for Exploring Electric-Field Control of Multifunctionalities <i>Jan-Chi Yang, Qing He, Pu Yu, and Ying-Hao Chu</i>	249
Citrate-Based Biomaterials and Their Applications in Regenerative Engineering <i>Richard T. Tran, Jian Yang, and Guillermo A. Ameer</i>	277
Corrosion of Zirconium Alloys Used for Nuclear Fuel Cladding <i>Arthur T. Motta, Adrien Couet, and Robert J. Comstock</i>	311
L1 ₂ -Strengthened Cobalt-Base Superalloys <i>Akane Suzuki, Haruyuki Inui, and Tresa M. Pollock</i>	345
Multiscale Simulation of Plasticity in bcc Metals <i>Daniel Weygand, Matous Mrovec, Thomas Hochrainer, and Peter Gumbsch</i>	369
An Overview of Dual-Phase Steels: Advances in Microstructure- Oriented Processing and Micromechanically Guided Design <i>C.C. Tasan, M. Diehl, D. Yan, M. Bechtold, F. Roters, L. Schemmann, C. Zheng, N. Peranio, D. Ponge, M. Koyama, K. Tsuzaki, and D. Raabe</i>	391
Polymer-Based Dielectrics with High Energy Storage Density <i>Qin Chen, Yang Shen, Shibai Zhang, and Q.M. Zhang</i>	433
The Power of Materials Science Tools for Gaining Insights into Organic Semiconductors <i>Neil D. Treat, Paul Westacott, and Natalie Stingelin</i>	459
Predicting and Designing Optical Properties of Inorganic Materials <i>James M. Rondinelli and Emmanouil Kioupakis</i>	491
Surface Engineering of Mo-Base Alloys for Elevated-Temperature Environmental Resistance <i>J.H. Perepezko</i>	519

Index

Cumulative Index of Contributing Authors, Volumes 41–45	543
---	-----

Errata

An online log of corrections to *Annual Review of Materials Research* articles may be found at <http://www.annualreviews.org/errata/matsci>